A *Tbx1-Six1/Eya1-Fgf8* genetic pathway controls mammalian cardiovascular and craniofacial morphogenesis

Chaoshe Guo, … , Anne Moon, Xue Li

Research Article Cardiology

Shared molecular programs govern the formation of heart and head during mammalian embryogenesis. Development of both structures is disrupted in human chromosomal microdeletion of 22q11.2 (del22q11), which causes DiGeorge syndrome (DGS) and velo-cardio-facial syndrome (VCFS). Here, we have identified a genetic pathway involving the Six1/Eya1 transcription complex that regulates cardiovascular and craniofacial development. We demonstrate that murine mutation of both *Six1* and *Eya1* recapitulated most features of human del22q11 syndromes, including craniofacial, cardiac outflow tract, and aortic arch malformations. The mutant phenotypes were attributable in part to a reduction of fibroblast growth factor 8 (Fgf8), which was shown to be a direct downstream effector of Six1 and Eya1. Furthermore, we showed that *Six1* and *Eya1* genetically interacted with *Fgf8* and the critical del22q11 gene T-box transcription factor 1 (*Tbx1*) in mice. Together, these findings reveal a *Tbx1-Six1/Eya1-Fgf8* genetic pathway that is crucial for mammalian cardiocraniofacial morphogenesis and provide insights into the pathogenesis of human del22q11 syndromes.

Find the latest version:

https://jci.me/44630/pdf

A *Tbx1-Six1/Eya1-Fgf8* genetic pathway controls mammalian cardiovascular and craniofacial morphogenesis

Chaoshe Guo,[1,2] Ye Sun,[1,2,3,4] Bin Zhou,[2,5] Rosalyn M. Adam,[1] XiaoKun Li,[3,4]
William T. Pu,[2,5] Bernice E. Morrow,[6] Anne Moon,[7] and Xue Li[1,2]

[1]Department of Urology, Children's Hospital Boston, and Department of Surgery and Pathology, Harvard Medical School, Boston, Massachusetts, USA.
[2]Harvard Stem Cell Institute, Cambridge, Massachusetts, USA. [3]School of Pharmaceutical Science, Wenzhou Medical College, Wenzhou, China.
[4]Norman Bethune College of Medicine, Jilin University, Changchun, China. [5]Department of Cardiology, Children's Hospital Boston, Harvard Medical School,
Boston, Massachusetts, USA. [6]Department of Genetics, Albert Einstein College of Medicine, New York, New York, USA. [7]Department of Pediatrics,
Department of Neurobiology and Anatomy, and Department of Human Genetics, Program in Molecular Medicine, University of Utah, Salt Lake City, Utah, USA.

Shared molecular programs govern the formation of heart and head during mammalian embryogenesis. Development of both structures is disrupted in human chromosomal microdeletion of 22q11.2 (del22q11), which causes DiGeorge syndrome (DGS) and velo-cardio-facial syndrome (VCFS). Here, we have identified a genetic pathway involving the Six1/Eya1 transcription complex that regulates cardiovascular and craniofacial development. We demonstrate that murine mutation of both *Six1* and *Eya1* recapitulated most features of human del22q11 syndromes, including craniofacial, cardiac outflow tract, and aortic arch malformations. The mutant phenotypes were attributable in part to a reduction of fibroblast growth factor 8 (Fgf8), which was shown to be a direct downstream effector of Six1 and Eya1. Furthermore, we showed that *Six1* and *Eya1* genetically interacted with *Fgf8* and the critical del22q11 gene T-box transcription factor 1 (*Tbx1*) in mice. Together, these findings reveal a *Tbx1-Six1/Eya1-Fgf8* genetic pathway that is crucial for mammalian cardiocraniofacial morphogenesis and provide insights into the pathogenesis of human del22q11 syndromes.

Introduction

Progenitors of the cardiac and craniofacial skeletal muscles arise from subdomains of a contiguous field of cephalic mesoderm: the ventrolateral primary heart field (PHF) and the dorsomedial cranial paraxial mesoderm (CPM), respectively. A distinct population of mesodermal progenitors located in between the PHF and CPM, called the secondary heart field (SHF), forms the cardiac outflow tract (OFT) and the RV in mammals (1–5). Recent studies demonstrated that genes critical for SHF development are also required for formation of the head branchiomeric muscles, which control jaw movement, facial expression, and pharyngeal functions (6, 7), and that head muscles and heart may a share common lineage (8). However, the molecular mechanisms that couple development of heart and face are poorly understood.

In humans, deletions of chromosome 22q11.2 cause del22q11 syndrome, DiGeorge syndrome (DGS), and velo-cardio-facial syndrome (VCFS). Affected patients exhibit a wide spectrum of developmental defects, including craniofacial anomalies, dysmorphogenesis of cardiovascular structures, and hypoplasia of the thymus and parathyroid glands (9, 10). Additionally, more than 30% of del22q11 patients have renal defects; however, the underlying etiology remains to be elucidated. T-box transcription factor 1 (*TBX1*) is located in the 22q11.2 critical region, and *TBX1* haploinsufficiency is a major contributor to human del22q11 phenotypes and to murine models of the syndrome (11, 12). Mouse *Tbx1* is expressed in SHF cardiac progenitors and is required for their proliferation as well as for cranial skeletal muscle development (13–17). Similar to human hemizygous

del22q11 phenotypes, mouse *Tbx1* haploinsufficiency causes aortic arch defects, whereas *Tbx1*-null mutants exhibit more severe cardiac and craniofacial anomalies (18–20).

Although human fibroblast growth factor 8 (*FGF8*) does not map to the 22q11.2 region, FGF8 and FGF signaling pathways are critical for cardiovascular development and have been directly implicated in the etiology of del22q11 syndromes (12, 21). Autocrine function of murine Fgf8 controls proliferation and survival of SHF cardiac progenitors (22, 23), whereas paracrine Fgf8 signals from the pharyngeal ectoderm and endoderm epithelia control formation and remodeling of both craniofacial structures and aortic arch arteries and cardiac OFT (13, 24–26). Double-heterozygous *Tbx1*^{+/–} *Fgf8*^{+/–} mutant embryos exhibit increased incidence of pharyngeal arch (PA) artery remodeling anomalies (27, 28), demonstrating a genetic link between *Tbx1* and *Fgf8* during vascular morphogenesis. Fgf8 activity has to be precisely controlled, as too much or too little is detrimental to cardiovascular development (29). For example, mutations of components of the Notch signaling pathway cause congenital heart defects in humans (30), which depends in part on modulation of *Fgf8* expression in the SHF (31). Fgf8 hypomorphic mice with reduced Fgf8 expression display a range of pharyngeal and cardiovascular phenotypes (32). Forced expression of *Fgf8* in a *Tbx1*-null background could not fully rescue the cardiac defects of *Tbx1*-null mutants and even increased the incidence of cardiovascular defects (28, 33). Despite the critical role of *Fgf8*, little is known about the direct transcriptional mechanism responsible for its gene regulation during cardiovascular development (14, 27, 34).

We reported previously that the evolutionarily conserved homeodomain transcription factor Six1 and its canonical coactivator Eya1 synergistically control organ-specific progenitor cell proliferation and survival (35). Deletion of either *Six1* or *Eya1* phe-
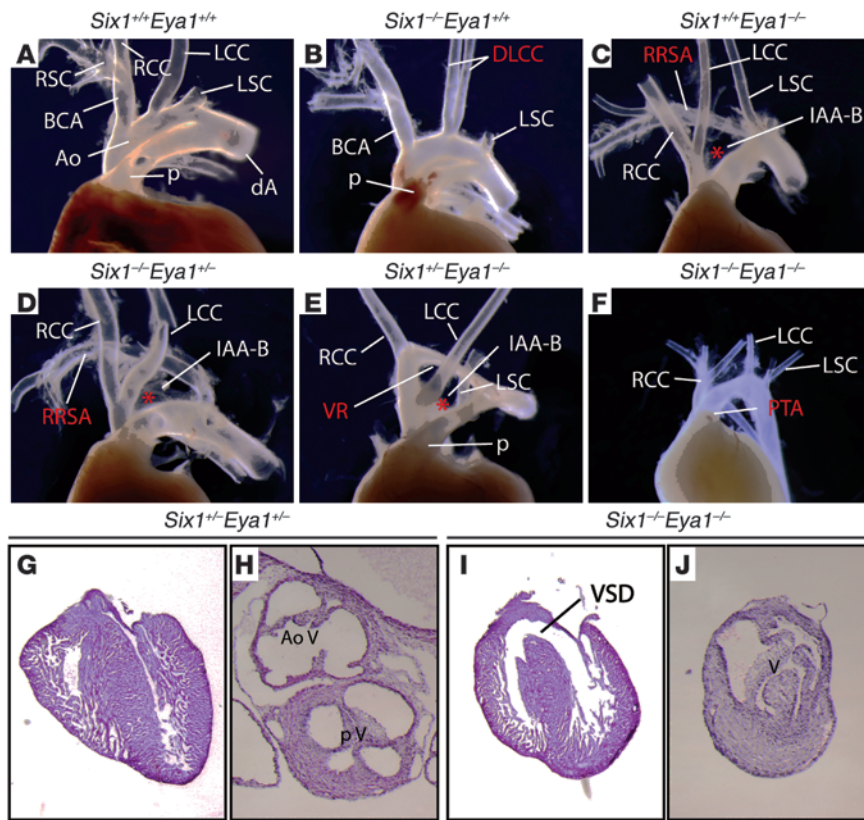
Figure 1
Six1⁻/⁻Eya1⁻/⁻ mutants phenocopy features of human del22q11 syndromes. (**A–F**) Gross morphological defects of the OFT and great arteries of newborn mutants (**B–F**) versus WT control (**A**). (**G–J**) H&E histological staining of sectioned hearts revealed VSD and dysmorphology of the outflow valves in a *Six1⁻/⁻Eya1⁻/⁻* mutant (**I** and **J**) compared with *Six1⁺/⁻Eya1⁺/⁻* control (**G** and **H**). Ao, aortic artery; BCA, brachiocephalic artery; dA, descending aorta; DLCC, duplicated left common carotid artery; LCC, left common carotid artery; LSC, left subclavian artery; p, pulmonary artery; RCC, right common carotid artery; RRSA, retroesophageal right subclavian artery; RSC, right subclavian artery; V, ventricle; VR, vascular ring. Asterisks denote interrupted aortic arches. Original magnification, ×50 (**G** and **I**); ×80 (**H** and **J**).

nocopies human branchio-oto-renal (BOR) syndrome, which is characterized by congenital preauricular pits, branchial fistulas, hearing loss, and renal agenesis (35–37). Human *EYA1* mutations are also found in patients with congenital cardiac abnormalities (38, 39). Mutation of the *EYA1* homolog *EYA4* causes dilated cardiomyopathy (40). Therefore, the Six1/Eya1 complex may have yet unidentified roles during cardiovascular development.

Here, we demonstrate that double-null *Six1⁻/⁻Eya1⁻/⁻* mutant mice exhibited phenotypes similar to *Tbx1* and *Fgf8* mouse mutants and phenocopied human del22q11 syndromes, including the major craniofacial and cardiovascular phenotypes. We provide genetic and molecular evidence indicating that a *Tbx1-Six1/Eya1-Fgf8* pathway is critical for morphogenesis of cardiocraniofacial structures and propose that mutations of *SIX1* and *EYA1* may contribute to the pathogenesis of both del22q11-like and BOR syndromes in humans.

Results

Six1 and Eya1 regulate cardiovascular and craniofacial morphogenesis. To determine a potential role of *Six1* and *Eya1* in cardiovascular development, we analyzed the cardiac phenotype of embryos with null mutation of 1 or both copies of *Six1* and *Eya1*. While *Six1⁺/⁻Eya1⁺/⁻* embryos had normal morphology of the aorta and pulmonary arteries, further loss of function of either *Six1* or *Eya1* caused a spectrum of abnormalities of great artery patterning (Figure 1 and Table 1) consistent with abnormal development of the PA arteries and characteristic of del22q11 syndromes (9, 10). For instance, 78% of *Eya1⁻/⁻* mutants had aortic arch defects (*n* = 13), including 54% with interrupted aortic arch type B (IAA-B), in which the transverse arch is disrupted between the left com-

mon carotid and left subclavian arteries. Other vascular anomalies found in *Eya1⁻/⁻* mutants included retroesophageal right subclavian artery (23%) and vascular ring (16%). *Six1⁻/⁻Eya1⁻/⁻* mutant embryos had a higher incidence and greater severity of cardiovascular phenotypes (Table 1). Instead of the normal OFT pattern, in which the aorta and pulmonary arteries connect to the LV and RV, respectively, 100% of *Six1⁻/⁻Eya1⁻/⁻* embryos exhibited OFT defects (*n* = 7). We found 14% had double-outlet RV (DORV), in which both great vessels arise from the RV, and egress of blood from the LV is via a ventricular septal defect (Figure 1I). Such defects were present in 100% of compound mutants. Approximately 70% of *Six1⁻/⁻Eya1⁻/⁻* mutants had a single, unseptated outflow vessel, and the outflow valve contained 3 or 4 leaflets (Figure 1J). These SHF-related defects are found in the human del22q11 patient population: persistent truncus arteriosus (PTA; a single unseptated OFT and outflow vessel reflecting failure of the embryonic truncus arteriosus to septate into 2 ventricular outflows); pulmonary atresia; tetralogy of Fallot; and, rarely, DORV (41, 42). They are also seen in animal models, including mouse mutants of *Tbx1* and *Fgf8* (13, 18–20, 22, 23, 25, 26, 43), manipulation of avian *Fgf8* expression (29), and SHF ablation in chicks (44).

In addition to cardiovascular defects, *Six1/Eya1* compound mutants exhibited a spectrum of craniofacial phenotypes, including micrognathia (small jaw) and cleft palate phenotypes found in human del22q11 patients (Supplemental Figure 1 and Supplemental Table 1; supplemental material available online with this article; doi:10.1172/JCI44630DS1) (9, 10, 35, 36, 45). *Six1⁻/⁻* mutants had micrognathia, dysmorphogenesis of the midface, and deformation of nasal structures (Supplemental Figure 1, A–F). *Eya1⁻/⁻* mutants had milder facial defects. Compound mutants exhibited progres-

Table 1
Six1 and *Eya1* synergistically regulate cardiovascular development

Genotype	n	Abnormal	IAA-B	RAA	RRSA	VR	DLCC	DORV	RAA and RPA	PTA
Six1+/−Eya1+/−	50	0%	0%	0%	0%	0%	0%	0%	0%	0%
Six1−/−Eya1+/+	20	5%[A]	0%	0%	0%	0%	5%[A]	0%	0%	0%
Six1+/+Eya1−/−	13	78%[B]	54%[B]	0%	23%[B]	16%[B]	0%	0%	0%	0%
Six1−/−Eya1+/−	15	87%[B]	33%[B]	27%[B]	20%[B]	0%	13%[A]	13%[A]	0%	0%
Six1+/−Eya1−/−	9	100%[B]	56%[B]	0%	44%[B]	11%[A]	0%	33%[B]	0%	0%
Six1−/−Eya1−/−	7	100%[B]	29%[B]	43%[B]	29%[B]	29%[B]	0%	14%[B]	14%[A]	71%[B,C]

DLCC, duplicated left common carotid artery; RAA, right-sided aortic arch; RPA, right-sided pulmonary artery; RRSA, retroesophageal right subclavian artery; VR, vascular ring. Statistical analyses were done by Fisher exact test. [A]No significant difference versus *Six1+/−Eya1+/−* control. [B]$P < 0.05$ versus *Six1+/−Eya1+/−* control. [C]$P < 0.05$ versus single-null mutants.

sively worse phenotypes, with the most severe defects found in the *Six1−/−Eya1−/−* mutants. To determine whether Six1 and Eya1 are part of the genetic program required for formation of both cardiac and branchiomeric skeletal muscles (6, 7), we examined all cranial skeletal muscles using an antibody marker, MF20 (myosin heavy chain–specific antibody) (Supplemental Figure 1, G–H). Similar to the mouse *Tbx1* mutant model of del22q11 syndromes (17), *Six1* and *Eya1* compound mutants had severely hypoplastic branchiomeric muscles. *Six1−/−Eya1−/−* mutants also had hypoplastic extraocular muscles, muscles of facial expression, and tongue. Thus, Six1 and Eya1 are required for both cardiovascular and craniofacial development.

Six1 is transiently expressed in a subset of cardiac progenitors. The surprising SHF-related OFT septation and alignment defects suggest a direct involvement of Six1 and Eya1 in the function of cardiac progenitors in the SHF. We therefore reexamined the early expression pattern of these genes during cardiogenesis, initially using a gene-specific RNA in situ hybridization approach (Supplemental Figures 2 and 3 and refs. 46, 47). At the cranial level, *Six1* and *Eya1* exhibited a lateromedial mesoderm expression gradient at E8.5: strong lateral expression in the CPM, faint but detectable expression in the SHF/splanchnic mesoderm (SHF/SpM), and undetectable expression in the PHF (Supplemental Figures 2 and 3). These findings indicated that *Six1* and *Eya1* are indeed expressed in the cardiac progenitors in the SHF/SpM. However, their signal intensities, a reflection of both gene expression level and sensitivity of the gene-specific probe, were considerably less than those of the known SHF progenitor marker genes *Tbx1* and islet LIM homeobox 1 (*Isl1*) (Supplemental Figures 2 and 3).

To better characterize the *Six1* expression pattern and cell lineages, we generated a *Six1Cre/hpAP* knockin/knockout mouse allele that expresses the Cre recombinase and a sensitive reporter, human placental alkaline phosphatase (hpAP). The dicistronic *Cre/hpAP* gene replaces and inactivates *Six1* using the same targeting strategy we reported previously (35). hpAP activity driven by this allele provided a surrogate for *Six1* expression and allowed us to better define the location, number, and fate of *Six1*-positive (*Six1+*) progenitors. We detected hpAP activity in the cardiogenic mesoderm at E7.5 (Figure 2, B–D), but not in the primitive heart tube at E8.5 (Figure 2, E and F) or in the heart at subsequent stages (data not shown). Consistent with the RNA in situ analysis (Supplemental Figures 2 and 3), we also detected strong endoderm staining as early as E7.5 and ectoderm staining at E8.5 (Figure 2, C and F). The hpAP activity was maintained in skeletal muscle and thymus, but absent from mature cardiac and renal tissues at later developmental stages (data not shown).

Six1+ progenitors contribute to multiple cardiac lineages. To determine whether *Six1+* progenitors contribute to mature cardiovascular tissues, we used double-heterozygous *Six1Cre/hpAPR26RmTmG* and *Six1Cre/hpAPR26RlacZ* embryos, in which *Six1+* progenitors and their progeny are permanently labeled with membrane-localized eGFP and β-gal reporters, respectively (Figure 2 and Supplemental Figure 4). eGFP+ cells were detected in the inflow tract and OFT of the looped heart at E9.0 (Figure 2, G–I), consistent with *Six1* expression in the SHF. This was further supported by colocalization of eGFP with the cardiac progenitor marker Isl1 (4, 48). Consistently, *Six1+* progenitors differentiated into multiple cell types, including ventricular cardiomyocytes and smooth muscle cells of the proximal aortic and pulmonary arteries, based on coimmunostaining with the cardiac-specific TNNT2 and ACTN2 and the smooth muscle–specific SM22α and CNN1 antibodies (49), respectively (Figure 2, J–N). In addition, eGFP colocalized with WT1 and RALDH2 (Figure 2O and Supplemental Figure 4, C–J), which suggests that *Six1* is expressed in epicardial progenitors (49–51). Thus, in addition to the previous reports of *Six1* expression in the pharyngeal ectoderm and endoderm, and the cranial skeletal muscle progenitors (35, 36), our detailed expression and fate-mapping analyses demonstrated that *Six1* was also expressed in cardiac progenitors in the SHF and proepicardium during cardiovascular development (Figure 2O). We posit that the combination of *Six1* and *Eya1* function in all these cells is required for normal cardiovascular and craniofacial morphogenesis.
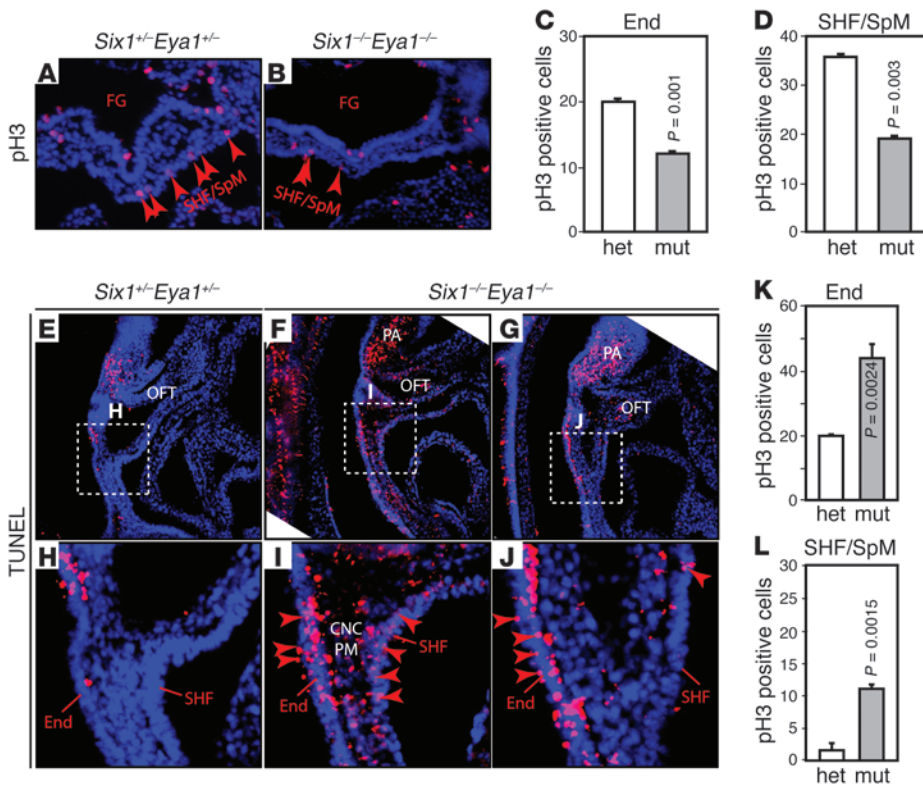
Six1 and Eya1 are required for cell survival and proliferation. We have shown previously that the Six1/Eya1 transcription complex is essential for renal progenitor cell survival and proliferation at E11.5 and E12.5 (35, 36, 52). Thus, we analyzed early-stage (E9.5 and E10.5) *Six1−/−Eya1−/−* mutants to determine whether a similar mechanism contributes to cardiovascular morphogenesis (Figure 3). We detected an approximately 50% reduction in phospho–histone H3–labeled (pH3-labeled) cells in the PAs and OFT of whole-mount and sectioned *Six1−/−Eya1−/−* specimens (Figure 3 and data not shown). Cardiac progenitors in the SHF/SpM had an approximately 48% reduction in pH3 labeling, and those in the foregut endoderm had an approximately 40% reduction (Figure 3, A–D). More apoptotic cells were detected in the SHF pharyngeal ectoderm and endoderm of the *Six1/Eya1* mutants relative to controls, based on both Lyso-Tracker and TUNEL staining (Figure 3, E–L, and data not shown). Thus, reduced proliferation and survival of the SHF and the pharyngeal ectoderm and endoderm epithelia in *Six1/Eya1* mutants likely contributes to the observed cardiovascular phenotypes, as has been reported in *Tbx1* and *Fgf8* mouse mutants with similar phenotypes.
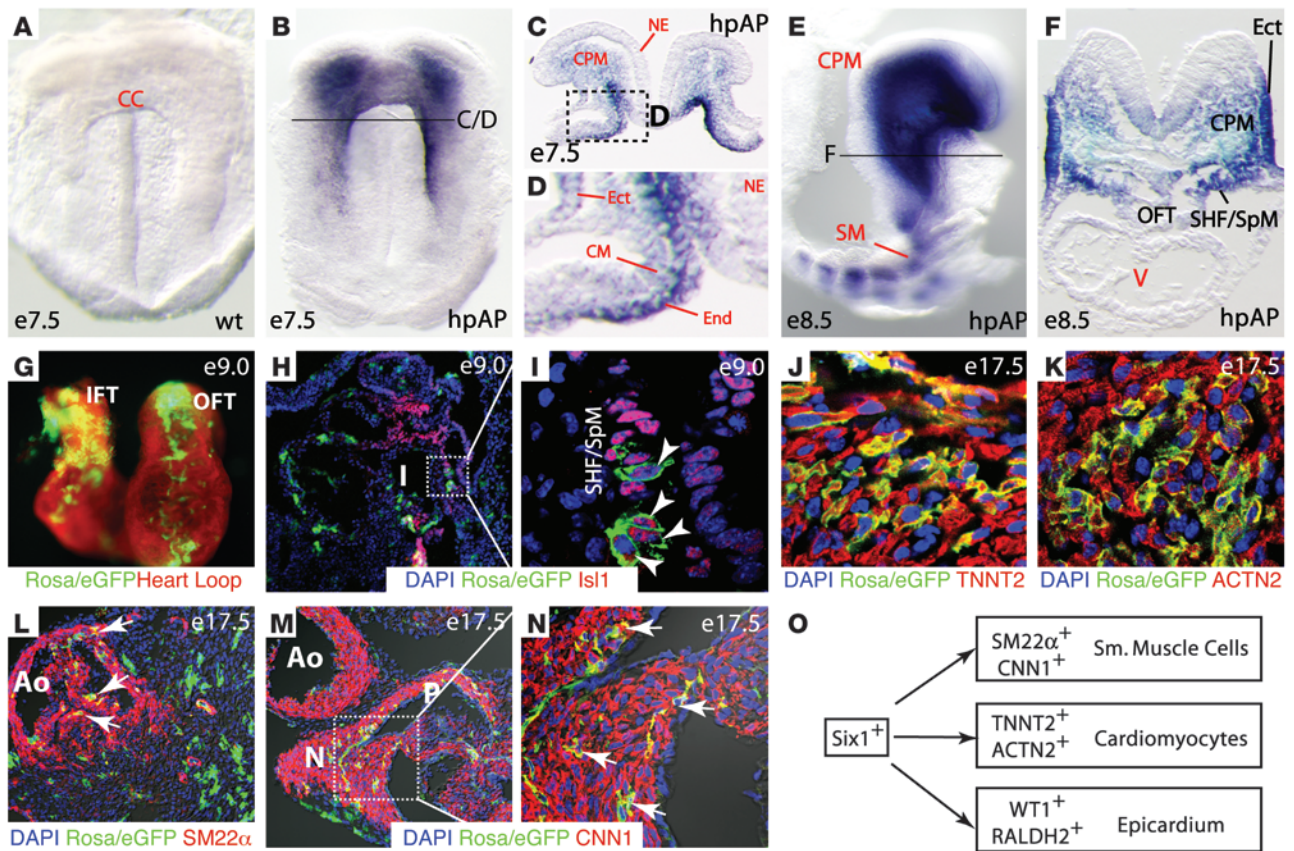
Figure 2

Six1 is expressed in cardiac progenitors. (**A–F**) *Six1* is expressed in cardiac/skeletal muscle progenitors and in cranial ectoderm and endoderm at E7.5 and E8.5. WT (**A**) and *Six1^{Cre/hpAP}* (**B–F**) embryos were stained for hpAP activity. Cross-sections of **B** are shown in **C** and **D**; cross-section of **E** is shown in **F**. CC, cardiac crescent; Ect, ectoderm; End, endoderm; NE, neural epithelium; SM, somite. (**G**) Whole-mount dorsal-right view of the looped heart from an E9.0 *Six1^{Cre/hpAP}R26R^{mTmG}* embryo. eGFP+ cells (Rosa/eGFP) in the *Six1* lineage were found in inflow tract (IFT), OFT, and developing apex. (**H** and **I**) eGFP+ cells in the *Six1* lineage and Isl1 colabeled SHF cardiac progenitor cells (arrowheads) in E9.0 sagittal sectioned tissue. Boxed region in **H** is enlarged in **I**. (**J–N**) Coimmunostaining of eGFP+ cells in the *Six1* lineage with TNNT2 (**J**) and ACTN2 (**K**) in the RV and with SM22α (**L**) and CNN1 (**M** and **N**, arrows) in the proximal region of the great arteries from E17.5 hearts. Boxed region in **M** is enlarged in **N**. Original magnification, ×115 (**A** and **B**); ×100 (**C**, **D**, and **F**); ×63 (**E**); ×200 (**G–N**). (**O**) Summary of Six1+ progenitor cell lineage, based on results from Figure 2 and Supplemental Figure 5 (WT1, RALDH2; epicardial progenitor data).

We also observed a substantial increase in apoptosis in the pharyngeal mesenchyme cells derived from either mesoderm or neural crests (Figure 3I). Defects of a specialized population of cardiac neural crest cells (CNCs) result in cardiovascular phenotypes similar to those found in the *Six1/Eya1* mutants (53–55). To analyze CNCs specifically, we examined the expression patterns of transcription factor AP-2α (*AP2*) and plexin A2 (*Plxna2*) (Supplemental Figure 5). These genes were detected in migrating CNCs in the mutant pharynx (*AP2*) and postmigratory CNCs in the mutant OFT (*Plxna2*) (Supplemental Figure 5). *AP2* expression in the ectoderm was unaffected (Supplemental Figure 5H), but staining in the caudal pharynx was decreased (Supplemental Figure 5, D and G, arrow). Consistent with a potential increase of CNC apoptosis (Figure 3I), the intensity of *Plxna2* staining in the prongs of CNCs invading the OFT appeared to be decreased (Supplemental Figure 5B), suggestive of fewer invading CNCs in the mutants. Together, these findings suggest that *Six1* and *Eya1* are required for CNC survival and that decreased CNC number and/or CNC dysfunction in the mutants may also contribute to the hypoplastic OFT cushions and septation failure.

Fgf8 expression depends on Six1 and Eya1 in vivo. To identify Six1/Eya1-dependent genetic pathways that regulate cardiovascular morphogenesis, we examined expression of a panel of molecular markers known to be important in SHF survival and function, including *Tbx1*, *Isl1*, *Fgf8*, and *Fgf10* (Figure 4 and Supplemental Figures 6–8). Of these genes, *Fgf8* exhibited a drastic reduction in expression throughout the PAs and the SHF at E9.5 in *Six1^{-/-}Eya1^{-/-}* mutants; expression levels of *Tbx1* and *Isl1* were unaltered despite the severe hypoplastic caudal arch defect (Figure 4, A–D and Supplemental Figures 6–8). Consistent with the gross cardiocraniofacial phenotypes (Figure 1), we noted that *Fgf8* expression in the caudal pharyngeal region and the SHF was more sensitive to the loss of *Eya1* than of *Six1*, and the reverse was true in the first arch (Figure 4, B and C). Similar to *Six1* and *Eya1*, *Fgf8* is required for SHF progenitor cell proliferation and survival (22, 23, 25, 26), and *Fgf8* mouse mutants display phenotypic features of del22q11 syndrome (32, 56). In contrast to *Tbx1* mutants, in which both *Fgf8* and *Fgf10* are reduced, expression of *Fgf10* in *Six1^{-/-}Eya1^{-/-}* mutants was slightly increased (Supplemental Figure 7). Baldini and col-

Figure 3

Six1 and *Eya1* are required for cell proliferation and survival in PA and OFT. (**A–D**) Anti-pH3 immunostaining (red) of E9.5 transverse sections to label proliferating cells. Quantification of results are shown in **C** and **D**. FG, foregut; mut, *Six1⁻/⁻Eya1⁻/⁻* mutant; het, heterozygous control. *n* = 3. (**E–L**) TUNEL staining of sagittal sections revealed increased cell death in pharyngeal endoderm, SHF/SpM, and pharyngeal mesenchyme (PM) that contained CNCs and mesoderm. Boxed regions in **E–G** are enlarged in **H–J**. Original magnification, ×200 (**A**, **B**, and **E–J**). *n* = 3. *P* values were determined by Student's *t* test.

leagues have demonstrated that *Tbx1* can directly regulate *Fgf10* in vitro (16), but it is not yet clear whether *Fgf8* is also a direct target of Tbx1 in some tissues (14). Our results suggest an alternate mechanism, in which Tbx1 may regulate *Fgf8* expression through the *Six1/Eya1* transcription complex.

The Six1/Eya1 transcription complex directly controls Fgf8 expression in vivo. To test whether Six1 and Eya1 directly control *Fgf8* gene expression, we first questioned whether they are expressed in the same cells. We used double-heterozygous *Six1^{hpAP/Cre/+}Fgf8^{eGFP/+}* embryos to address this question. Expression of *eGFP* in these embryos depends on the endogenous promoter activity of both *Fgf8* and *Six1* and therefore can be used as a sensitive indicator of the same cell lineages (25). *Six1^{hpAP/Cre/+}Fgf8^{eGFP/+}* embryos displayed strong Fgf8/eGFP expression in the pharyngeal region and the cardiac OFT (Figure 4E), which is similar to previously reported *Fgf8/eGFP* activity (25). These Fgf8/eGFP⁺ lineages included Nkx2.5⁺ cells in the bulbus cordis and the conotruncus (which contribute to the RV and OFT, respectively; Figure 4, F and G) and Isl1⁺ cells in the pharyngeal endoderm and ectoderm and the SHF/SpM (Figure 4, H and I). Furthermore, Fgf8/eGFP colocalized with Six1/Cre immunoreactivity in the SHF/SpM and pharyngeal endoderm (Figure 4, J and K), which suggests that *Six1* and *Fgf8* are coexpressed in multiple cell lineages.

To examine whether Six1/Eya1 can directly regulate *Fgf8* expression, we analyzed a genomic fragment containing an *Fgf8* enhancer sufficient to drive transgene reporter expression in pharyngeal ectoderm and endoderm and in cardiac OFT (14). The proximal *Fgf8* promoter has 3 conserved regions in mice, rats, cows, and primates, and we identified 4 putative *Six1* binding sites distributed among those 3 regions (Figure 4L). The second and third sites were clustered in the second conserved region (~130 bp). A *luciferase* reporter driven by

a 2.4-kb mouse *Fgf8* enhancer fragment had negligible activity after transient transfection in HEK293 cells. Cotransfection of either *Six1* or *Eya1* resulted in a 3-fold increase in reporter activity, and there was synergistic enhancement of the reporter activity to approximately 13-fold when both factors were present (Figure 4M). Because truncation analyses indicated that the second conserved region (Fgf8-d) had relatively higher activity than the first and third regions (Figure 4N), we focused on the 2 putative Six1-binding sites within the second conserved region. Mutation of these 2 sites significantly decreased reporter activity (Figure 4O). To confirm that Six1 binds directly to the endogenous *Fgf8* enhancer, we purified Six1-associated chromatin from E9.5 mouse embryonic PAs and cardiac tissues. Real-time quantitative PCR analyses indicated that binding of Six1 to the endogenous *Fgf8* enhancer was enriched more than 4-fold relative to the coding region of *Fgf8* and IgG control (Figure 4P). Together, these findings strongly suggest that the Six1/Eya1 transcription complex directly regulates *Fgf8* gene expression in vivo.

To further establish the functional relationship in vivo between Six1 and *Fgf8*, we analyzed compound *Six1^{Cre/hpAP}–Fgf8^{f/+}* mutants (ref. 32 and Supplemental Figure 9). In these mutants, a single allele of *Fgf8* is inactivated specifically in *Six1*-expressing cells. *Six1⁻/⁻* and *Six1^{Cre/hpAP/+}Fgf8^{f/+}* mutants had only rare great vessel defects (Table 2); however, 83% of *Six1^{Cre/hpAP}–Fgf8^{f/+}* mutants exhibited IAA-B or cervical aortic arch phenotypes. This functional interaction strongly suggests that *Six1* and *Fgf8* are in the same genetic pathway and synergistically regulate cardiovascular morphogenesis. Decreased expression of *Fgf8* likely contributes to the observed del22q11-like phenotypes in *Six1⁻/⁻Eya1⁻/⁻* mutants.

Exogenous Fgf8 rescues endothelial-to-mesenchymal transformation defects. Fgf8 signaling is critical for endothelial-to-mesenchymal transformation (EMT) in the proximal OFT cushions and for
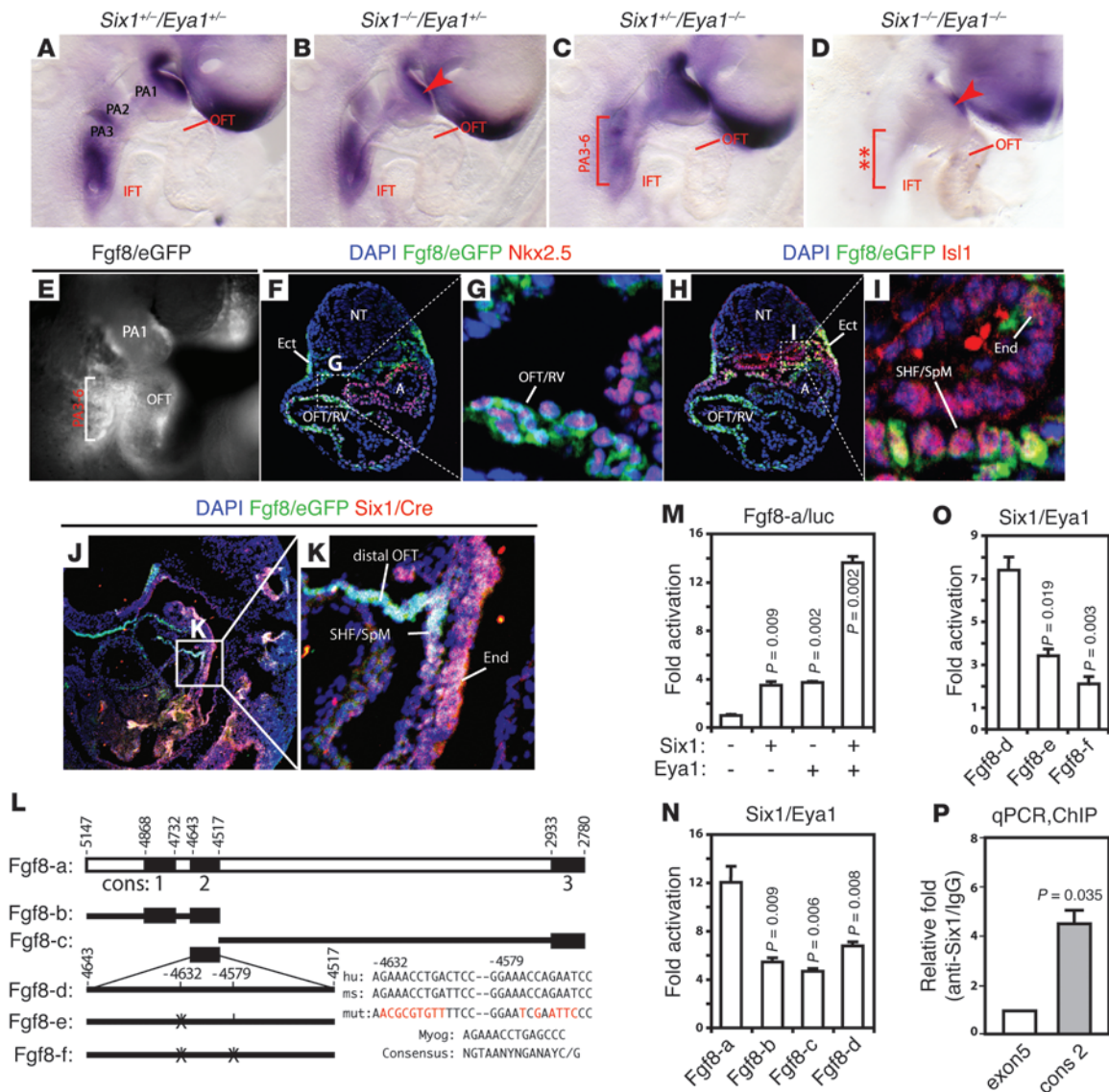
Figure 4
Six1 and *Eya1* directly regulate *Fgf8* expression. (**A–D**) *Fgf8* expression was dependent on *Six1* and *Eya1*. *Fgf8* was downregulated in the PA ectoderm (arrowhead) of E9.5 *Six1⁻/⁻Eya1⁺/⁻* (**B**) and *Six1⁻/⁻Eya1⁻/⁻* (**D**) mutants and other PA regions (bracket) of *Six1⁺/⁻Eya1⁻/⁻* (**C**) and *Six1⁻/⁻ Eya1⁻/⁻* (**D**) mutants. (**E–I**) *Six1hpAP/Cre* efficiently turned on the *Fgf8eGFP* reporter allele in the pharynx (**E**, bracket) and OFT. eGFP⁺ (Fgf8/eGFP) cells were found in the pharyngeal ectoderm (**F**), endoderm (**I**), SHF/SpM (**I**), and OFT/RV (**F** and **G**). eGFP staining colocalized with Nkx2.5 in the OFT/RV (**F** and **G**) and Isl1 in the SHF/SpM (**G** and **I**). A, atrium; NT, neural tube. (**J** and **K**) Colabeling of *Six1*-expressing cells with Cre antibody (red) and *Fgf8*-expressing cells with eGFP antibody (green) of E9.5 *Six1hpAP/CreFgf8eGFP* embryos (sagittal section). Colabeling appeared white with blue DAPI counter staining. Boxed regions in, **F**, **H**, and **J** are enlarged in **G**, **I**, and **K**, respectively. Original magnification, ×100 (**A–D**); ×200 (**E–K**). (**L**) Potential murine *Fgf8* enhancer. Dark boxes mark evolutionarily conserved regions (cons); putative *Six1* binding sites and mutations (red) are listed. hu, human; ms, mouse. (**M–O**) Six1 and Eya1 synergistically regulated reporters containing WT *Fgf8* enhancers (**M** and **N**), but not the putative *Six1* binding site mutant enhancers (**O**), in transiently transfected HEK293 cells. Reporter constructs are as in **L**. (**P**) Quantitative PCR analyses of in vivo ChIP assays of E9.5 mouse PA/heart tissues. Six1 protein was selectively bound to the second conserved region of *Fgf8* enhancers (cons2; ~4.4-fold relative to anti-Six1/IgG enrichment). *Fgf8* coding region (exon5) served as a negative control.

CNC migration and invasion of both proximal and distal OFT cushions (26, 31). Consistently, we found that *Six1⁻/⁻Eya1⁻/⁻* mutants had severely hypoplastic proximal and distal OFT cushions compared with WT littermate controls (Figure 5, A–H). Using an established OFT explant culture assay (26, 31, 57), we found that both *Six1⁺/⁻Eya1⁻/⁻* and *Six1⁻/⁻Eya1⁻/⁻* mutants had a dramatic reduction in the number of mesenchymal cells that

invaded the gel and migrated away from the beating myocardial explants (Figure 5, I–P). These results suggest that the Six1/Eya1 complex is required indirectly through Fgf8 for EMT of OFT endothelial cells during cushion remodeling.

To determine whether Fgf8 is sufficient to rescue EMT in *Six1⁺/⁻ Eya1⁻/⁻* mutant phenotypes, we treated WT and mutant explants with recombinant Fgf8 isoform b protein (rFgf8b) or BSA control

Table 2

Six1 and *Fgf8* are in the same genetic pathway

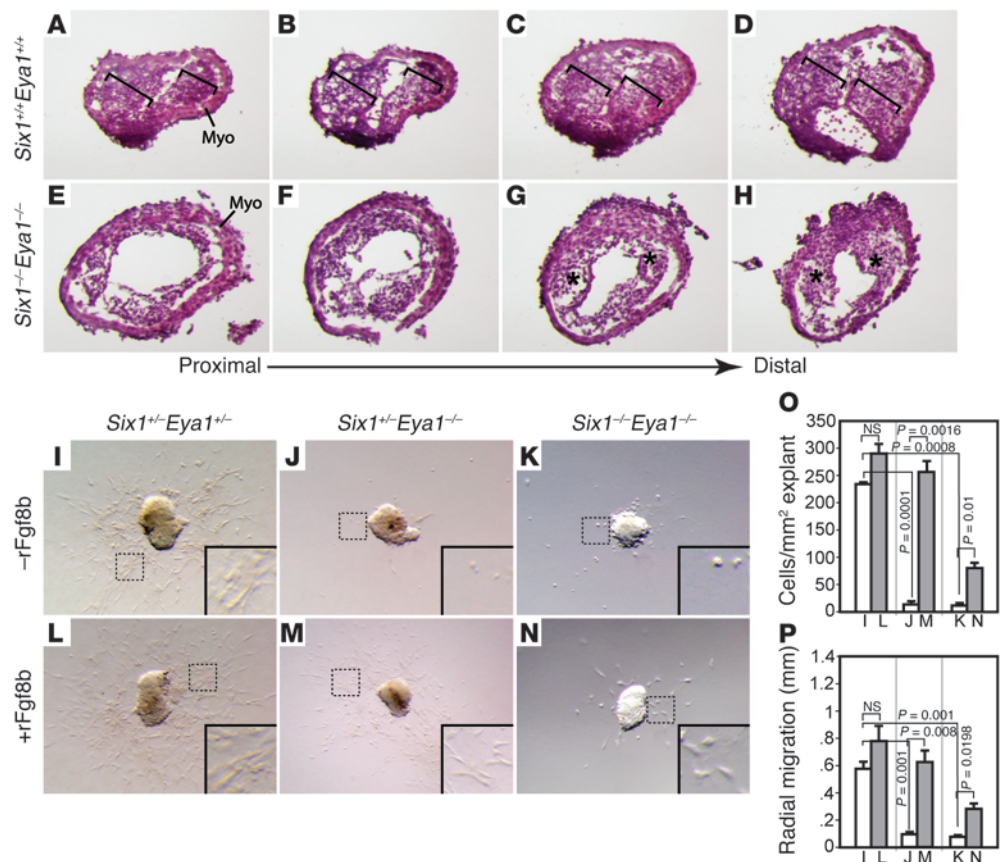| Genotype	n	Abnormal	IAA-B	RRSA	VR
Six1⁻/⁻	20	5%	0%	0%	0%
Six1^{Cre/hpAP/+}Fgf8^{f/+}	8	0%	0%	0%	0%
Six1^{Cre/hpAP/−}Fgf8^{f/+}	6	83%[A]	83%[A]	33%[B]	67%[A]

RRSA, retroesophageal right subclavian artery; VR, vascular ring. Statistical analyses were done by Fisher exact test. [A]$P < 0.05$. [B]No significant difference.

and assayed EMT by counting the total number of mesenchymal cells that invaded the gel as well as the distance migrated from the explant after invasion. Whereas very few mesenchymal cells were present in untreated compound mutant explants and the few present had not migrated far (Figure 5J), rFgf8b treatment almost fully rescued EMT and migration defects of *Six1⁺/⁻Eya1⁻/⁻* mutants (Figure 5, I–P). The *Six1⁻/⁻Eya1⁻/⁻* mutant phenotypes were also rescued, but to a lesser extent, indicating, not surprisingly, that additional factors downstream of Six1/Eya1 contribute to defects in the *Six1⁻/⁻Eya1⁻/⁻* mutant.
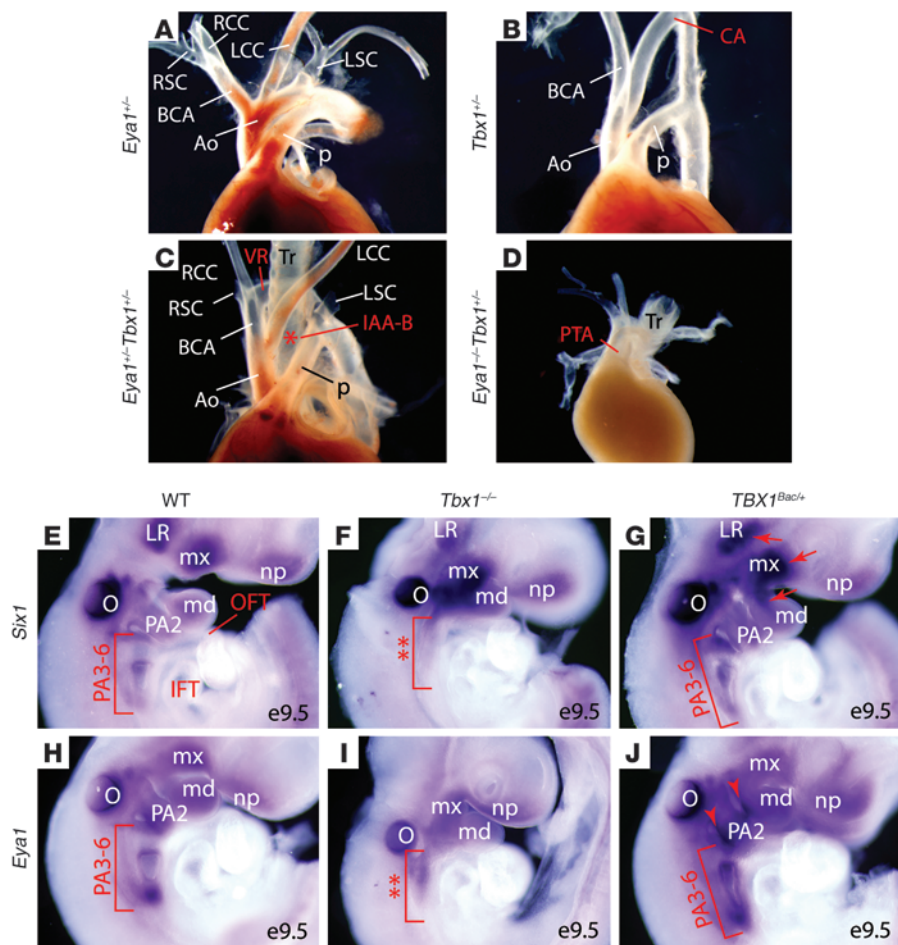
Tbx1 is a genetic upstream regulator of Six1 and Eya1. Although human *SIX1* and *EYA1* do not map to chromosome 22q11.2, the shared morphological defects and molecular phenotype of decreased *Fgf8* expression in *Six1/Eya1* and *Tbx1* mutant mouse models suggests that human *SIX1* and *EYA1* may be genetic modifiers of the del22q11 syndrome. To test this possibility using mouse models, we examined the functional relationship between *Six1* or *Eya1* and *Tbx1* by analyzing compound mutants of these genes in a C57BL6/CD-1 mixed genetic background (Figure 6, A–D, and Table 3). Whereas 25% of *Tbx1⁺/⁻* mutants (*n* = 12) had cardiovascular defects at E17.5, none of the *Eya1⁺/⁻* mutants did (*n* > 10). Penetrance of these defects increased to 73% in *Eya1⁺/⁻Tbx1⁺/⁻* mutants (*n* = 15). Remarkably, although approximately 80% of *Eya1⁻/⁻* mutants had cardiovascular phenotypes (*n* = 13), none of them had the severe defect of a single outflow vessel seen in *Tbx1⁻/⁻* mutants, in contrast to 100% of *Eya1⁻/⁻Tbx1⁺/⁻* mutants (*n* = 5; Figure 6D

and Table 3). Similar to *Eya1/Tbx1* compound mutants, 63% of *Six1⁻/⁻Tbx1⁺/⁻* mutants (*n* = 8) had cardiovascular phenotypes, in contrast to less than 5% of *Six1⁻/⁻* mutants (*n* = 20) and 33% of *Tbx1⁺/⁻* mutants (*n* = 9). Together, these findings demonstrated that *Six1*, *Eya1*, and *Tbx1* are in a common genetic pathway controlling cardiovascular and craniofacial development.

Since *Tbx1* expression in the pharyngeal epithelia appeared to be unaffected in *Six1⁻/⁻Eya1⁻/⁻* mutants (Supplemental Figures 7 and 8), we next examined the possibility that *Six1* and *Eya1* function downstream of Tbx1. Both *Six1* and *Eya1* were downregulated in the presumptive caudal arch tissue (PA3–PA6 region) of *Tbx1* mutants (Figure 6, F and I). It is not clear whether the observed reduction of *Six1* and *Eya1* expression in *Tbx1* mutants is attributable to arch hypoplasia and failed segmentation (i.e., fewer cells to express the genes), or rather reflects a direct effect of *Tbx1* loss of function on expression of these genes (i.e., less expression in affected cells). We reasoned that if *Six1* and *Eya1* are genetically downstream of Tbx1, increased levels of Tbx1 should result in their upregulation. We therefore examined transgenic mice that overexpress human *TBX1*

Figure 5

Fgf8 rescues EMT defects in *Six1/Eya1* mutant OFT explants. (**A–H**) *Six1⁻/⁻Eya1⁻/⁻* mutants (**E–H**) had hypoplastic OFT cushions compared with WT littermate controls (**A–D**). Shown are serial histological sections of E11.5 outflow vessels proceeding from proximal (**A** and **E**) to distal (**D** and **H**). Brackets in **A–D** indicate WT OFT cushions, which were hypoplastic in the mutants (asterisks). Myo, myocardium. (**I–K**) The compound mutants (**J** and **K**) had fewer endothelial cells migrating from the OFT explant, undergoing EMT, and invading the gel than did WT controls (**I**) in cultured E9.5 OFTs. (**L–N**) The EMT defect was rescued by rFgf8b in the explant culture. Original magnification, ×230 (**A–H**); ×100 (**I–N**). (**O** and **P**) Quantification of results in **I–N**. White bars, without rFgf8b; gray bars, with rFgf8b. Student's *t* test. *n* = 6 (control); 3 (*Six1⁺/⁻Eya1⁻/⁻* and *Six1⁻/⁻Eya1⁻/⁻*).

Figure 6
Eya1 functionally interacts with Tbx1 in vivo. (**A–D**) Gross views of cardiovascular structures of newborn *Eya1/Tbx1* compound mutants. Asterisk in **C** denotes interrupted aortic arches. (**E–J**) Whole-mount RNA in situ hybridization revealed altered *Six1* and *Eya1* expression in *Tbx1⁻/⁻* (**F** and **I**) and *TBX1^{Bac/+}* gain-of-function mutants (**G** and **J**). *Tbx1⁻/⁻* mutants had hypoplastic and unsegmented caudal PAs (**F** and **I**, double asterisks). Brackets in **G** and **J** indicate increased expression of *Six1* and *Eya1* in the *TBX1* gain-of-function mutants. Arrows in **G** denote *Six1* upregulation. Arrowheads in **J** indicate enhanced *Eya1* expression. CA, cervical aortic arch; LR, lateral rectus muscle; md, mandible; mx, maxillary; np, nasal placode; O, otic vesicle; Tr, trachea. Original magnification, ×63 (**E–J**).

using a BAC (20). As expected, 54% of the transgenic mice had vascular defects involving the aortic arch and/or great vessels in the face of relatively normal morphology of the pharyngeal apparatus (20, 58, 59). We noted enhanced expression of both *Six1* and *Eya1* in the PA3–PA6 region (Figure 6, G and J). *Six1*, but not *Eya1*, was also upregulated in pharyngeal mesoderm (Figure 6G, arrows), including primordium of the lateral rectus eye muscle and the first branchial arch core mesoderm. *Eya1* expression in the pharyngeal epithelia, particularly in the pharyngeal clefts, was increased in *TBX1^{Bac/+}* transgenic mice (Figure 6J, arrowheads). Together, these loss-of-function and gain-of-function analyses revealed a functional relationship in which *Tbx1* is genetically upstream of *Six1* and *Eya1* during cardiocraniofacial morphogenesis. It remains to be determined whether Tbx1 directly regulates *Six1* and *Eya1* gene expression in vivo.

Discussion

Here, we uncovered what we believe to be a novel function for the Six1/Eya1 transcription complex in cardiovascular development and delineated a *Tbx1-Six1/Eya1-Fgf8* regulatory cascade that controls morphogenesis of mammalian heart and face. Our findings suggest that dysregulation of this molecular pathway is likely to be a critical mechanism underlying the pathogenesis of del22q11-like syndromes in humans.

The present study provides evidence that *Six1* is transiently expressed in cardiac progenitors in the SHF and proepicardium and contributes directly to cardiovascular development. The restricted distribution pattern of *Six1* progeny, which is reminiscent of the SHF in chicks (3), suggests that *Six1* is expressed in a subpopulation of the SHF lineages marked by Isl1 or Tbx1 (4, 60). It is also possible, however, that the lineage tracing experiments may be limited by inefficient recombination rate as a result of weak enhancer activity of the endogenous *Six1* locus in these cells. We showed that *Six1* and *Eya1* were broadly expressed in the pharyngeal ectoderm, endoderm, and mesoderm (including SHF). Consequently, deletion of both genes resulted in downregulation of *Fgf8* in all 3 cell layers, all of which are likely to contribute to the observed morphological defects of cardiocraniofacial structures (21, 24, 25). Future conditional knockout experiments will be needed to define the tissue-specific roles of Six1/Eya1.

Six1⁻/⁻Eya1⁻/⁻ mutants had a single unseptated OFT in addition to other typical vascular defects seen in del22q11 human patients (Figure 1). It has been proposed that the lesion diagnosed as PTA in some cases of human del22q11 and animal models of this syndrome may in fact be a severe form of pulmonary atresia in which the entire RV outflow fails to form, resulting in a single outflow vessel that is the aorta (43, 61). However, at this point, the morphological and molecular criteria for this important distinction remain to be established. Based on the variable and abnormal outflow valve morphology and the size and location of the outflow vessel in *Six1⁻/⁻Eya1⁻/⁻* mutants, we think the defect is likely PTA, but recognize the possibility that the spectrum of defects in these mutants may include pulmonary atresia.

Table 3

Eya1 functionally interacts with *Tbx1* in vivo

Genotype	n	Abnormal	IAA-B	RRSA	VR	CA	PTA
Eya1+/–	>10	0%	0%	0%	0%	0%	0%
Tbx1+/–	12	25%	8%	17%	0%	8%	0%
Eya1+/–Tbx1+/–	15	73.3%[A]	26.7%	46.7%	6.7%	13.3%	0%
Eya1–/–	13	78%	54%	23%	16%	0%	0%
Eya1–/–Tbx1+/–	5	100%	0%	40%	0%	0%	100%[A]

CA, cervical aortic arch; RRSA, retroesophageal right subclavian artery; VR, vascular ring. Statistical analyses were done by Fisher exact test. [A]$P < 0.05$.

To our knowledge, no direct in vivo transcriptional regulator of *Fgf8* has previously been described. Loss of *Tbx1* causes a significant reduction of both *Fgf8* and *Fgf10*, which may have redundant roles during cardiovascular development (12, 14, 16, 21, 27, 62). *Fgf10* in the SHF, but not *Fgf8*, is a direct downstream target of Tbx1 (1, 14, 16). Hu et al. demonstrated that Tbx1 is required for an orthologous region upstream of the human *FGF8* locus to enhance reporter activity in the OFT of transgenic mice; expression of the enhancer in the PAs (including SHF) was not affected by loss of Tbx1 (14). Furthermore, mutation of 3 putative Tbx1 binding sites found in the *FGF8* enhancer did not affect its activity in vivo. Thus, it is unclear whether *Tbx1* directly activates *Fgf8* in vivo. We found that *Tbx1* expression was unaltered in the *Six1–/–Eya1–/–* mutants (Supplemental Figures 6–8), despite the severe morphological caudal arch defects. Both *Six1* and *Eya1* were reduced in *Tbx1–/–* loss-of-function mutants and enhanced in the *Tbx1Bac/+* gain-of-function transgenics (Figure 6). Tbx1 may therefore be genetic upstream of *Six1* and *Eya1*. Furthermore, we demonstrated that *Six1* and *Fgf8* were coexpressed in the pharyngeal ectoderm and endoderm and in some cardiac progenitors in the SHF. *Fgf8*, but not *Fgf10*, was severely reduced in all these cells in the *Six1–/–Eya1–/–* mutants (Figure 4 and Supplemental Figure 7). We showed that not only did *Six1/Eya1* compound mutants share cardiovascular and craniofacial features with *Fgf8* mutants, they synergistically interacted to regulate pharyngeal artery patterning, which strongly suggests that they are in the same genetic pathway. Taken together, our results indicate that the Six1/Eya1 transcription complex directly controls *Fgf8* expression through an evolutionarily conserved enhancer element (Figure 4). Future studies will determine whether Tbx1 is a direct regulator of *Six1* and Eya1.

Recent studies in *Drosophila melanogaster* demonstrate that the fly *eya1* ortholog is a direct downstream target of *tinman*. Nkx2.5, the mammalian ortholog of *tinman*, is required for both PHF and SHF development (63, 64). In *Drosophila*, *eya1* and *tinman* are initially coexpressed throughout the mesoderm, after which their localization becomes mutually exclusive, with *eya* restricted to ventral mesoderm and *tinman* present only dorsally. *tinman* is also required for *Drosophila* expression of *six4* and differentiation of muscle along the dorsoventral axis (65). In addition, zebrafish *six1* and *eya1* were reported to function downstream of *tbx1* during craniofacial myogenesis (66). Thus, an evolutionarily conserved network consisting of *Tbx1*, *Nkx2.5*, *Six1*, and *Eya1* may be critical for specification and differentiation of cranial skeletal and cardiac muscle.

Haploinsufficiency of *SIX1* and *EYA1* in humans causes BOR syndrome (35, 36), which often exhibits kidney and ear anomalies but does not routinely feature cardiovascular defects. It is important to note that frequent and severe cardiovascular defects were found only in *Six1–/–Eya1–/–* mutant mice (Table 1). Renal defects

are seen in nearly one-third of del22q11 patients (9, 10, 41, 42), but *Tbx1*-null mutants do not exhibit any apparent renal defects (18–20). Thus, *TBX1* haploinsufficiency is unlikely to be the genetic basis for the renal defects in affected human del22q11 patients. In contrast, *Six1* and *Eya1* were critical regulators of kidney development (Supplemental Table 1 and refs. 35, 52). We hypothesize that mutations of human *SIX1* and *EYA1* likely contribute to the pathogenesis of del22q11 syndrome and that the pathogenesis of human BOR and del22q11-like syndromes may be linked.

Methods

Knockout mice and histological analyses. Six1Cre/hpAP was generated using the same targeting strategy as previously described (35). *Six1/Eya1* compound mutants were generated by crossing *Six1+/–* and *Eya1+/–* mice (36), and all mutants were confirmed by PCR. *Fgf8eGFP*, *Fgf8f/f*, *R26RlacZ*, and *R26RmTmG*Cre reporter mice were reported previously (20, 25, 32, 67). All mice were maintained on C57BL6, 129svj, or CD-1 mixed genetic backgrounds. Heads, hearts, and aortic arch arteries were dissected, embedded in OCT, sectioned, and stained with H&E using standard procedures. All animal studies were performed according to protocols reviewed and approved by the Institutional Animal Care and Use Committee at the Children's Hospital Boston.

Gene expression analyses. Whole-mount RNA in situ hybridization with digoxigenin-UTP–labeled riboprobes and specific gene probes was performed as previously described (35, 67–69). For quantitative PCR analyses, relative gene expression levels were normalized to a GAPDH internal control from the E9.5 pharynx and heart, analyzed using the SYBR Green method on an ABI-7500 detector (Applied BioSystems).

Immunohistochemistry and TUNEL assay. Staged embryos were dissected, fixed in 4% paraformaldehyde for 1–2 hours at 4°C, and then sectioned at 8–10 μm. Anti-PECAM1 (BD Biosciences), cardiac Troponin T (Thermo scientific), WT1, NKX2-5, GATA4 (Santa Cruz Biotech), ISLET1 (DSHB), GFP (Rockland), Calponin, SM22α (Abcam), and cardiac α-actin (Sigma-Aldrich) were all incubated at 1:100 in blocking solution, except for anti-pH3 (Upstate), which was incubated at 1:200. TUNEL assay was performed on cryostat sections according to the manufacturer's instructions (Roche). The number of pH3+ or TUNEL+ cells was averaged from 3 sections per embryo. In total, 3 embryos per genotype were quantified.

Whole-mount and section β-galactosidase and hpAP staining. As described previously (35, 68), we detected β-galactosidase activity and hpAP activity in whole-mount embryos using X-gal and BM purple substrate, respectively.

In vivo ChIP. ChIP was performed as described previously (67, 70). PAs and cardiovascular tissues from 40 E9.5 embryos were used for each ChIP experiments. Normal serum (IgG) and nonspecific *Fgf8* intragenic region were used as negative controls. Anti-Six1 antibody (Sigma-Aldrich) specific oligos for real-time PCR reactions were as follows: Fgf8 promoter (con2) forward, 5′-CTGTGAGGGGTGGGGACCAGTC-3′; Fgf8 promoter (con2) reverse, 5′-CGAGGTTGATTCCCAGGGGCTC-3′; Fgf8 negative control (exon5) forward, 5′-ACGGCGCTGCAGAACGCCAAG-3′; Fgf8 negative control (exon5) reverse, 5′-CAGGCTCTGCTCGGTGGTGTG-3′. 3 independent ChIPs with triplicate real-time PCR reactions were performed per experiment.

Luciferase reporter assays. HEK293 cells were transfected with the designated plasmids (100 ng/plasmid/well, 24-well plate) using Lipofectamine 2000 (Invitrogen). Transfected cells were collected and lysed 48 hours after transfection with 50 mM Tris-MES, pH 7.8; 1 mM DTT; and 0.1% Triton X-100. The resulting cell lysates were measured using a Sirius Single Tube Luminometer (Berthold Detection Systems) according to the manufacturer's instructions. Results represent 3 independent assays, each having 3 replicates.

OFT explant culture. The OFT explants were cultured as previously described (26, 31, 57). OFTs of E9.5 embryos were microdissected and divided into halves along the longitudinal axis from proximal to distal. For the rescue experiments, 50 ng/ml mouse rFgf8b (R&D Systems) or vehicle solution (0.1% mg/ml BSA in PBS) was added. Cell migration distance from the edge of the explant was measured at 8 different locations every 45° and then averaged. The number of migrating cells was normalized to the explant area. Data represent 3 independent experiments.

Statistics. Paired 2-tailed Student's *t* test was used for data analysis between groups for qRT-PCR, pH3 and TUNEL staining, in vivo ChIP, reporter assay, and OFT explant culture. Data are presented as mean ± SEM (*n* = 3). Phenotypic data were analyzed with Fisher exact test. *P* values less than 0.05 were considered statistically significant.

Address correspondence to: Xue (Sean) Li, Room 1061.4, Enders Research Building, Children's Hospital Boston, Harvard Medical School, 300 Longwood Ave., Boston, Massachusetts 02115, USA. Phone: 617.919.2703; Fax: 617.730.0530; E-mail: sean.li@childrens.harvard.edu.

Bin Zhou's present address is: Institute for Nutritional Sciences, Shanghai Institutes for Biological Sciences, Chinese Academy of Sciences, and Graduate School of the Chinese Academy of Sciences, Shanghai, China.

1. Kelly RG, Brown NA, Buckingham ME. The arterial pole of the mouse heart forms from Fgf10-expressing cells in pharyngeal mesoderm. *Dev Cell*. 2001;1(3):435–440.
2. Mjaatvedt CH, et al. The outflow tract of the heart is recruited from a novel heart-forming field. *Dev Biol*. 2001;238(1):97–109.
3. Waldo KL, et al. Conotruncal myocardium arises from a secondary heart field. *Development*. 2001;128(16):3179–3188.
4. Cai CL, et al. Isl1 identifies a cardiac progenitor population that proliferates prior to differentiation and contributes a majority of cells to the heart. *Dev Cell*. 2003;5(6):877–889.
5. Dodou E, Verzi MP, Anderson JP, Xu SM, Black BL. Mef2c is a direct transcriptional target of ISL1 and GATA factors in the anterior heart field during mouse embryonic development. *Development*. 2004;131(16):3931–3942.
6. Grifone R, Kelly RG. Heartening news for head muscle development. *Trends Genet*. 2007;23(8):365–369.
7. Tzahor E. Heart and craniofacial muscle development: a new developmental theme of distinct myogenic fields. *Dev Biol*. 2009;327(2):273–279.
8. Lescroart F, Kelly RG, Le Garrec JF, Nicolas JF, Meilhac SM, Buckingham M. Clonal analysis reveals common lineage relationships between head muscles and second heart field derivatives in the mouse embryo. *Development*. 2010;137(19):3269–3279.
9. Lindsay EA. Chromosomal microdeletions: dissecting del22q11 syndrome. *Nat Rev Genet*. 2001;2(11):858–868.
10. Kobrynski LJ, Sullivan KE. Velocardiofacial syndrome, DiGeorge syndrome: the chromosome 22q11.2 deletion syndromes. *Lancet*. 2007;370(9596):1443–1452.
11. Paylor R, Lindsay E. Mouse models of 22q11 deletion syndrome. *Biol Psychiatry*. 2006;59(12):1172–1179.
12. Aggarwal VS, Morrow BE. Genetic modifiers of the physical malformations in velo-cardio-facial syndrome/DiGeorge syndrome. *Dev Disabil Res Rev*. 2008;14(1):19–25.
13. Chen L, Fulcoli FG, Tang S, Baldini A. Tbx1 regulates proliferation and differentiation of multipotent heart progenitors. *Circ Res*. 2009;105(9):842–851.
14. Hu T, Yamagishi H, Maeda J, McAnally J, Yamagishi C, Srivastava D. Tbx1 regulates fibroblast growth factors in the anterior heart field through a reinforcing autoregulatory loop involving forkhead transcription factors. *Development*. 2004;131(21):5491–5502.
15. Zhang Z, Huynh T, Baldini A. Mesodermal expression of Tbx1 is necessary and sufficient for pharyngeal arch and cardiac outflow tract development. *Development*. 2006;133(18):3587–3595.
16. Xu H, et al. Tbx1 has a dual role in the morphogenesis of the cardiac outflow tract. *Development*. 2004;131(13):3217–3227.
17. Kelly RG, Jerome-Majewska LA, Papaioannou VE. The del22q11.2 candidate gene Tbx1 regulates branchiomeric myogenesis. *Hum Mol Genet*. 2004;13(22):2829–2840.
18. Jerome LA, Papaioannou VE. DiGeorge syndrome phenotype in mice mutant for the T-box gene, Tbx1. *Nat Genet*. 2001;27(3):286–291.
19. Lindsay EA, et al. Tbx1 haploinsufficieny in the DiGeorge syndrome region causes aortic arch defects in mice. *Nature*. 2001;410(6824):97–101.
20. Merscher S, et al. TBX1 is responsible for cardiovascular defects in velo-cardio-facial/DiGeorge syndrome. *Cell*. 2001;104(4):619–629.
21. Rochais F, Mesbah K, Kelly RG. Signaling pathways controlling second heart field development. *Circ Res*. 2009;104(8):933–942.
22. Park EJ, et al. Required, tissue-specific roles for Fgf8 in outflow tract formation and remodeling. *Development*. 2006;133(12):2419–2433.
23. Ilagan R, et al. Fgf8 is required for anterior heart field development. *Development*. 2006;133(12):2435–2445.
24. Trumpp A, Depew MJ, Rubenstein JL, Bishop JM, Martin GR. Cre-mediated gene inactivation demonstrates that FGF8 is required for cell survival and patterning of the first branchial arch. *Genes Dev*. 1999;13(23):3136–3148.
25. Macatee TL, Hammond BP, Arenkiel BR, Francis L, Frank DU, Moon AM. Ablation of specific expression domains reveals discrete functions of ectoderm- and endoderm-derived FGF8 during cardiovascular and pharyngeal development. *Development*. 2003;130(25):6361–6374.
26. Park EJ, et al. An FGF autocrine loop initiated in second heart field mesoderm regulates morphogenesis at the arterial pole of the heart. *Development*. 2008;135(21):3599–3610.
27. Vitelli F, Taddei I, Morishima M, Meyers EN, Lindsay EA, Baldini A. A genetic link between Tbx1 and fibroblast growth factor signaling. *Development*. 2002;129(19):4605–4611.
28. Vitelli F, Zhang Z, Huynh T, Sobotka A, Mupo A, Baldini A. Fgf8 expression in the Tbx1 domain causes skeletal abnormalities and modifies the aortic arch but not the outflow tract phenotype of Tbx1 mutants. *Dev Biol*. 2006;295(2):559–570.
29. Hutson MR, et al. Cardiac arterial pole alignment is sensitive to FGF8 signaling in the pharynx. *Dev Biol*. 2006;295(2):486–497.
30. High FA, Epstein JA. The multifaceted role of Notch in cardiac development and disease. *Nat Rev Genet*. 2008;9(1):49–61.
31. High FA, et al. Murine Jagged1/Notch signaling in the second heart field orchestrates Fgf8 expression and tissue-tissue interactions during outflow tract development. *J Clin Invest*. 2009;119(7):1986–1996.
32. Frank DU, et al. An Fgf8 mouse mutant phenocopies human 22q11 deletion syndrome. *Development*. 2002;129(19):4591–4603.
33. Vitelli F, Lania G, Huynh T, Baldini A. Partial rescue of the Tbx1 mutant heart phenotype by Fgf8: genetic evidence of impaired tissue response to Fgf8. *J Mol Cell Cardiol*. 2010;49(5):836–840.
34. Lania G, et al. Early thyroid development requires a Tbx1-Fgf8 pathway. *Dev Biol*. 2009;328(1):109–117.
35. Li X, et al. Eya protein phosphatase activity regulates Six1-Dach-Eya transcriptional effects in mammalian organogenesis. *Nature*. 2003;426(6964):247–254.
36. Xu PX, Adams J, Peters H, Brown MC, Heaney S, Maas R. Eya1-deficient mice lack ears and kidneys and show abnormal apoptosis of organ primordia. *Nat Genet*. 1999;23(1):113–117.
37. Ruf RG, et al. SIX1 mutations cause branchio-oto-renal syndrome by disruption of EYA1-SIX1-DNA complexes. *Proc Natl Acad Sci U S A*. 2004;101(21):8090–8095.
38. Shimasaki N, Watanabe K, Hara M, Kosaki K. EYA1 mutation in a newborn female presenting with cardiofacial syndrome. *Pediatr Cardiol*. 2004;25(4):411–413.
39. Taylor MH, Wilton NC. Bradycardia with sevoflurane in siblings with Branchio-oto-renal syndrome. *Paediatr Anaesth*. 2007;17(1):80–83.
40. Schonberger J, et al. Mutation in the transcriptional coactivator EYA4 causes dilated cardiomyopathy and sensorineural hearing loss. *Nat Genet*. 2005;37(4):418–422.
41. Derbent M, Yilmaz Z, Baltaci V, Saygili A, Varan B, Tokel K. Chromosome 22q11.2 deletion and phenotypic features in 30 patients with conotruncal heart defects. *Am J Med Genet A*. 2003;116A(2):129–135.
42. Robin NH, Shprintzen RJ. Defining the clinical spectrum of deletion 22q11.2. *J Pediatr*.

2005;147(1):90–96.

43. Theveniau-Ruissy M, et al. The del22q11.2 candidate gene Tbx1 controls regional outflow tract identity and coronary artery patterning. *Circ Res*. 2008;103(2):142–148.

44. Ward C, Stadt H, Hutson M, Kirby ML. Ablation of the secondary heart field leads to tetralogy of Fallot and pulmonary atresia. *Dev Biol*. 2005;284(1):72–83.

45. Zou D, Silvius D, Davenport J, Grifone R, Maire P, Xu PX. Patterning of the third pharyngeal pouch into thymus/parathyroid by Six and Eya1. *Dev Biol*. 2006;293(2):499–512.

46. Xu PX, Woo I, Her H, Beier DR, Maas RL. Mouse Eya homologues of the Drosophila eyes absent gene require Pax6 for expression in lens and nasal placode. *Development*. 1997;124(1):219–231.

47. Oliver G, et al. Homeobox genes and connective tissue patterning. *Development*. 1995;121(3):693–705.

48. Moretti A, et al. Multipotent embryonic isl1+ progenitor cells lead to cardiac, smooth muscle, and endothelial cell diversification. *Cell*. 2006;127(6):1151–1165.

49. Zhou B, et al. Epicardial progenitors contribute to the cardiomyocyte lineage in the developing heart. *Nature*. 2008;454(7200):109–113.

50. Cai CL, et al. A myocardial lineage derives from Tbx18 epicardial cells. *Nature*. 2008;454(7200):104–108.

51. Christoffels VM, Grieskamp T, Norden J, Mommersteeg MT, Rudat C, Kispert A. Tbx18 and the fate of epicardial progenitors. *Nature*. 2009; 458(7240):E8–E9.

52. Xu PX, Zheng W, Huang L, Maire P, Laclef C, Silvius D. Six1 is required for the early organogenesis of mammalian kidney. *Development*. 2003;

130(14):3085–3094.

53. Hutson MR, Kirby ML. Neural crest and cardiovascular development: a 20-year perspective. *Birth Defects Res C Embryo Today*. 2003;69(1):2–13.

54. Hutson MR, Kirby ML. Model systems for the study of heart development and disease. Cardiac neural crest and conotruncal malformations. *Semin Cell Dev Biol*. 2007;18(1):101–110.

55. Stoller JZ, Epstein JA. Cardiac neural crest. *Semin Cell Dev Biol*. 2005;16(6):704–715.

56. Abu-Issa R, Smyth G, Smoak I, Yamamura K, Meyers EN. Fgf8 is required for pharyngeal arch and cardiovascular development in the mouse. *Development*. 2002;129(19):4613–4625.

57. Camenisch TD, Schroeder JA, Bradley J, Klewer SE, McDonald JA. Heart-valve mesenchyme formation is dependent on hyaluronan-augmented activation of ErbB2-ErbB3 receptors. *Nat Med*. 2002;8(8):850–855.

58. Zhang Z, Baldini A. In vivo response to high-resolution variation of Tbx1 mRNA dosage. *Hum Mol Genet*. 2008;17(1):150–157.

59. Liao J, et al. Full spectrum of malformations in velo-cardio-facial syndrome/DiGeorge syndrome mouse models by altering Tbx1 dosage. *Hum Mol Genet*. 2004;13(15):1577–1585.

60. Huynh T, Chen L, Terrell P, Baldini A. A fate map of Tbx1 expressing cells reveals heterogeneity in the second cardiac field. *Genesis*. 2007;45(7):470–475.

61. Kirby ML. Pulmonary atresia or persistent truncus arteriosus: is it important to make the distinction and how do we do it? *Circ Res*. 2008;103(4):337–339.

62. Watanabe Y, Miyagawa-Tomita S, Vincent SD, Kelly RG, Moon AM, Buckingham ME. Role of mesoder-

mal FGF8 and FGF10 overlaps in the development of the arterial pole of the heart and pharyngeal arch arteries. *Circ Res*. 2010;106(3):495–503.

63. Liu YH, Jakobsen JS, Valentin G, Amarantos I, Gilmour DT, Furlong EE. A systematic analysis of Tinman function reveals Eya and JAK-STAT signaling as essential regulators of muscle development. *Dev Cell*. 2009;16(2):280–291.

64. Prall OW, et al. An Nkx2-5/Bmp2/Smad1 negative feedback loop controls heart progenitor specification and proliferation. *Cell*. 2007;128(5):947–959.

65. Clark IB, Boyd J, Hamilton G, Finnegan DJ, Jarman AP. D-six4 plays a key role in patterning cell identities deriving from the Drosophila mesoderm. *Dev Biol*. 2006;294(1):220–231.

66. Lin CY, Chen WT, Lee HC, Yang PH, Yang HJ, Tsai HJ. The transcription factor Six1a plays an essential role in the craniofacial myogenesis of zebrafish. *Dev Biol*. 2009;331(2):152–166.

67. Olson LE, et al. Homeodomain-mediated beta-catenin-dependent switching events dictate cell-lineage determination. *Cell*. 2006;125(3):593–605.

68. Li X, Perissi V, Liu F, Rose DW, Rosenfeld MG. Tissue-specific regulation of retinal and pituitary precursor cell proliferation. *Science*. 2002; 297(5584):1180–1183.

69. Zhou W, et al. Modulation of morphogenesis by noncanonical Wnt signaling requires ATF/CREB family-mediated transcriptional activation of TGF-beta2. *Nat Genet*. 2007;39(10):1225–1234.

70. Giordani J, Bajard L, Demignon J, Daubas P, Buckingham M, Maire P. Six proteins regulate the activation of Myf5 expression in embryonic mouse limbs. *Proc Natl Acad Sci U S A*. 2007;104(27):11310–11315.